

The role of seismic intensity on the performance of caisson foundations supporting bridge piers: preliminary results from dynamic centrifuge testing

Domenico Gaudio, Ph.D.¹, Sebastiano Rampello, Ph.D.
Sapienza University of Rome

Gopal S.P. Madabhushi, Ph.D, Giulia M.B. Viggiani, Ph.D
University of Cambridge

ABSTRACT

Seismic performance of caisson foundations supporting bridge piers may take advantage of soil inelastic response when subjected to strong seismic events, thanks to the soil nonlinear and hysteretic behaviour. This can bring to a substantial optimisation in caisson design and major cost savings. In the framework of *Capacity Design* extended to geotechnical systems, temporary attainment of plastic mechanisms may be permitted provided that the resulting permanent displacements are lower than given threshold values, which in turn depend on the considered limit state and performance level required to the structure. Clearly, this new design approach needs to be validated against physically-sound numerical and experimental simulations. A campaign of dynamic centrifuge tests was therefore recently carried out at the Schofield Centre, University of Cambridge, where the seismic performance of caisson foundations was assessed. In this paper, a preliminary interpretation of the experimental results is given, shedding some light on the interplay between seismic intensity and mechanical soil properties. Specifically, the results obtained in two tests are discussed, where a caisson-pier-deck system was subjected to earthquakes of increasing intensity. In the two tests, a soft and very soft clay layer was reproduced, to either avoid or promote the plastic soil behaviour. It is shown that the highly nonlinear and hysteretic response of the very soft clay limits the inertial forces transmitted to the superstructure, thus validating the above-mentioned design approach. The beneficial effect of inelastic soil behaviour entailed permanent displacements increasing with earthquake intensity, which should be checked against limit state prescriptions.

Keywords: caisson foundations, bridge piers, earthquakes, centrifuge modelling

INTRODUCTION

In the presence of strong seismic shakings, inelastic soil behaviour is typically mobilised. However, current code provisions do not allow the soil-foundation system to fall in the elastic-plastic regime, while development of plastic hinges in the superstructure is allowed. Even if there are good reasons for this choice (e.g., post-earthquake inspection of the foundation is usually unfeasible), this design approach requires some overstrength factors to be applied in the foundation design, thus introducing a sort of overdesign (Gazetas, 2015). Furthermore, this approach may be even dangerous for the superstructure, as this may be subjected to a high ductility demand (Sakellariadis *et al*, 2020). Hence, plastic mechanisms occurring in the foundation soils may be promoted to limit the inertial forces transmitted to the superstructure, leading to substantial cost savings when either designing or retrofitting the structures at hand. Although attractive, this design procedure needs

¹ Department of Structural and Geotechnical Engineering, e-mail: domenico.gaudio@uniroma1.it;
formerly Department of Engineering, University of Cambridge, CB3 0EF, Cambridge, UK

the consequent displacements and rotations experienced by the structure to be checked, aiming at lying below given threshold values, which in turn depend on the considered limit state and on the performance level required to the structure.

Gaudio & Rampello (2019a, b; 2021) recently showed that the above-mentioned concept may be successfully applied in the design of caisson foundations supporting bridge piers. Their results were obtained by performing 3D Finite Element numerical analyses in the time domain: hence, dynamic centrifuge tests on reduced-scale models were recently carried out at the Schofield Centre, University of Cambridge, on the purpose of validating the numerical results, understanding the physical phenomena underlying the seismic performance and providing an experimental dataset for possible macro-element calibration.

In this paper, a preliminary interpretation of the experimental outcomes is given, stressing out the interplay between the seismic intensity and mechanical soil characteristics. Figure 1 shows the problem layout, in which a cylindrical caisson foundation of diameter $D = 8$ m and slenderness ratio $H/D = 1$ is embedded in a typical alluvial deposit, made by a thin sand layer ($H_1 = 3$ m) underlain by a soft or very soft clay deposit ($H_2 = 14$ m).

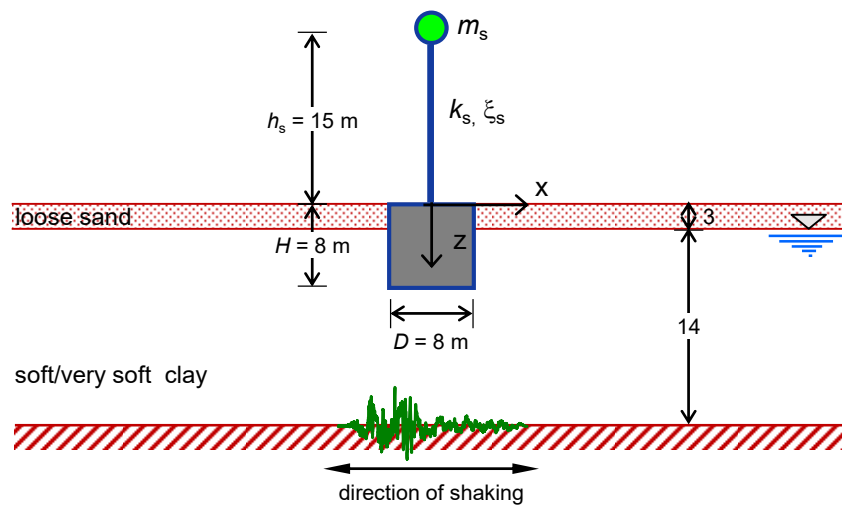


Figure 1. Schematic layout of the problem (prototype scale)

The water table is located at the sand-clay interface and the pore water pressure regime is hydrostatic. The pier is represented by a Single Degree of Freedom (SDoF) system with a height $h_s = 15$ m: its mechanical properties (lumped mass m_s and stiffness k_s) were back-calculated to provide a given average contact pressure, $q = 140$ kPa, and a fixed-based period, $T_s = 0.50$ s, both representative of a typical bridge configuration. The seismic input is applied in terms of a horizontal acceleration time history at the bedrock depth ($z = 17$ m), here assumed as infinitely rigid and therefore acting as a fully-reflecting boundary.

The results obtained in two out of three dynamic centrifuge tests are discussed in this paper, namely DG01 and DG03, the former characterised by a caisson-pier system resting on a soft clay, the latter on a very soft clay layer. Although the schematic layout considered in the centrifuge is not exactly the same as in the numerical analyses, the experimental layout allowed to validate the applicability of the numerical results to different soil-caisson-pier configurations.

CENTRIFUGE MODELLING

A reduced-scale model was produced to simulate the problem layout on the Turner beam centrifuge of the Schofield Centre at University of Cambridge, UK. The centrifuge model was prepared and spun at a nominal centrifugal acceleration of 60g.

The model container used was the most recent Equivalent Shear Beam (ESB) container (Brennan & Madabhushi, 2002): reliability of this container in dynamic centrifuge testing has been recently shown and discussed (Gaudio *et al.*, 2022a). The caisson foundation was simulated through a hollow aluminium cylinder

topped by two circular aluminium plates, while the pier was modelled using an aluminium rod with a squat brass cylinder at the top to reproduce the mass of the deck. At the model scale, the caisson is characterised by a diameter of 133 mm, equal to its depth, while the pier height is equal to 250 mm (Fig. 2). The hole into the caisson foundation was introduced to reproduce the mass of a concrete caisson ($m_{\text{caisson}} = 4.74 \cdot 10^{-3}$ Mg, corresponding to 1024.8 Mg at prototype scale), while the superstructure is reproduced by the brass mass $m_{\text{deck}} = 0.9 \cdot 10^{-3}$ Mg (194.4 Mg) and the pier, the latter characterised by a mass $m_{\text{pier}} = 0.665 \cdot 10^{-3}$ Mg (143.6 Mg) and a bending stiffness $EI = 2.37 \cdot 10^{-6}$ GN·m² (30.7 GN·m²). Hostun sand HN31, available at the Schofield Centre, was glued on the lateral surface of the caisson foundation to reproduce the roughness of the soil-concrete contact (Fig. 3a).

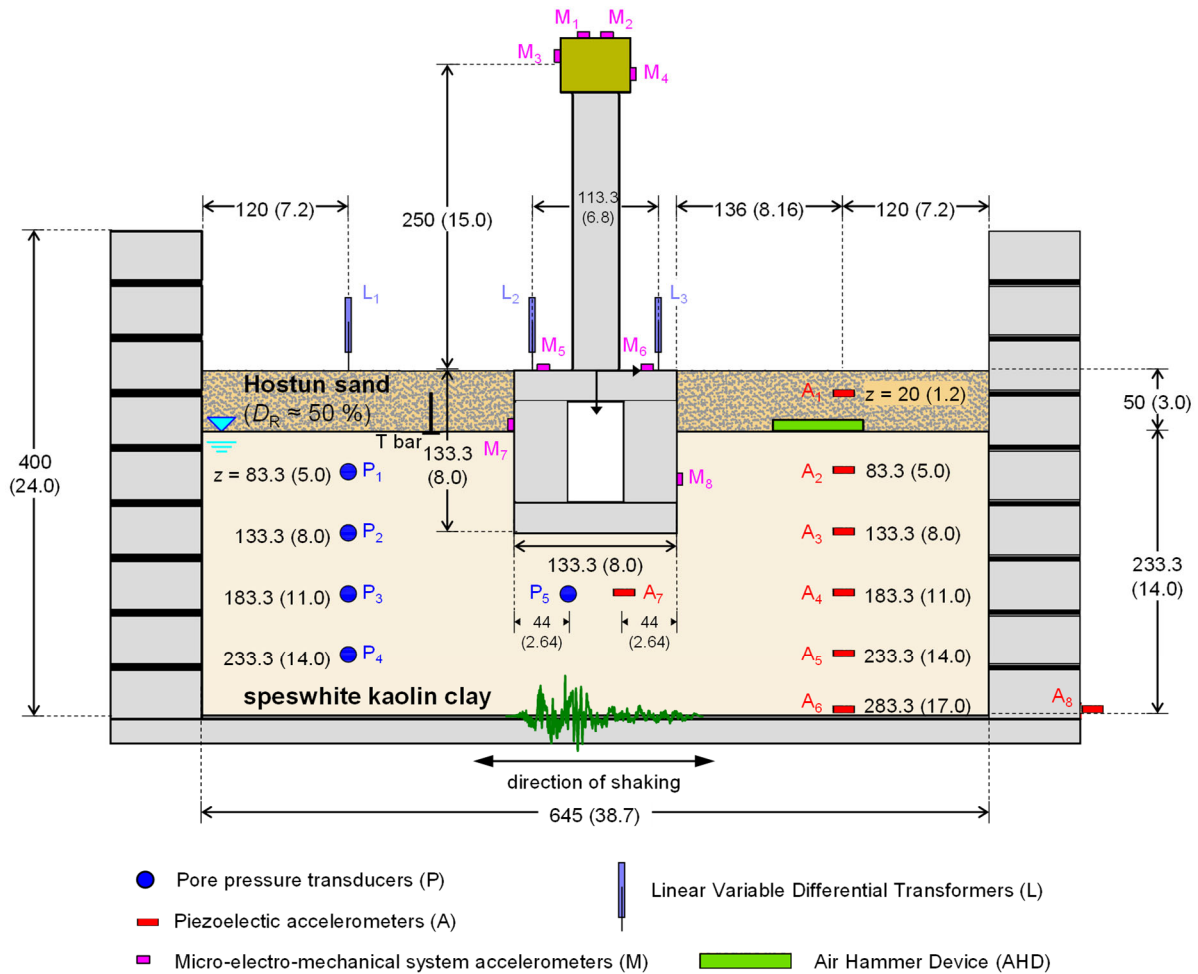


Figure 2. Cross-sectional view of the reduced-scale model and miniaturized instrumentation – model scale in mm (bracketed prototype scale in m)

The soil deposit was produced in two steps. First, the clay slurry was prepared by mixing speswhite kaolin clay powder and de-aired water in 1:1.3 ratio, and then the slurry was poured into the ESB box. Two different profiles of undrained shear strength s_u were targeted, both slightly increasing with depth, as for soft clays, and with average values equal to about 40 kPa (test DG01) and 10 kPa (DG03). The desired profiles were obtained via a combination of 1D loading and hydraulic consolidation by suction-induced seepage (Garala & Madabhushi, 2019) and are plotted in the following (Fig. 4b). After consolidating, the clay surface was trimmed to obtain the desired depth of 233 mm (Fig. 2) and the instrumentation was inserted in the model. The structure was then installed and the clay was covered with a layer of loose sand (relative density $D_R \approx 50\%$). The instrumentation includes two far-field alignments of miniature Pore Pressure Transducers (PPTs, P_{1-4} in Fig. 2) and piezo-electric accelerometers (A_{1-6}): two piezo-electric accelerometers were also installed at the outer base of the ESB container to record the applied seismic input (A_{8-9} , with A_9 not shown in the Figure as located out of plane), while PPT P_5 and piezo-electric accelerometer A_7 were installed beneath the caisson

base. Horizontal and vertical acceleration time histories were recorded by Micro-Electro-Mechanical-Systems (*MEMS*) glued on the brass mass (M_{1-4}) and on the caisson (M_{5-8}), whereas the average settlement and rigid rotation of the caisson were measured using two Linear Variable Differential Transformers *LVDTs* (L_{2-3}). Another *LVDT* (L_1) was installed at the clay surface along the far-field alignment to record vertical displacements. The model was also equipped with the *Air Hammer Device* (AHD; Ghosh & Madabhushi, 2002) and *T-bar* penetrometer (Stewart & Randolph, 1984) to measure the shear wave velocity and the undrained shear strength of the soil, respectively; the *T-bar* location is also given in the picture of the model mounted on centrifuge reported in Figure 3b. Both the *AH* and *T-bar* tests were performed at 60g to obtain the soil stiffness and strength right before the earthquakes were applied.

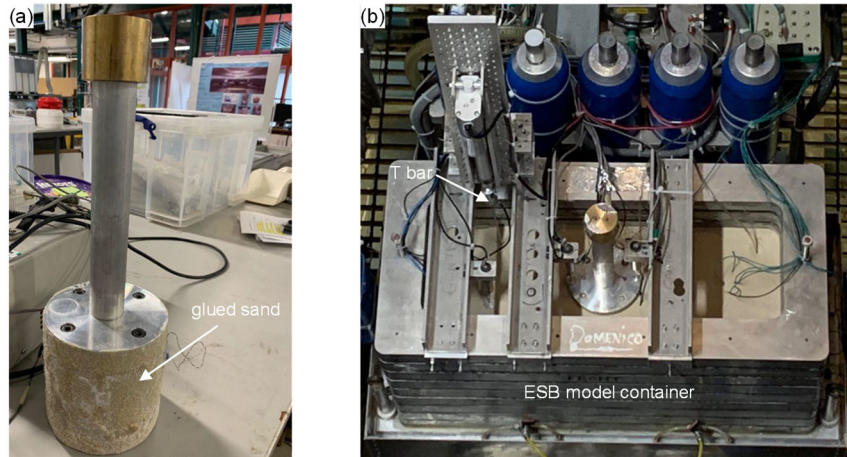


Figure 3. (a) system considered in the centrifuge tests DG01 and DG03; (b) model mounted in the centrifuge

The experimental profiles of the small-strain shear modulus G_0 and undrained shear strength s_u are plotted in Figure 4, the former computed through the well-known equation for an elastic medium

$$G_0(z) = \rho \cdot [V_{s,0}(z)]^2 \quad (1)$$

where ρ is the mass density and $V_{s,0}$ is the “small-strain” shear wave velocity. The undrained shear strength of the clay layer was obtained from the following relation:

$$s_u(z) = \frac{q_c(z)}{N_T} \quad (2)$$

where q_c is the penetration resistance and $N_T = 12$ is the *T-bar* bearing factor which was calibrated against the results from miniaturised shear vane tests (Gaudio *et al*, 2022b). As for the small-strain shear modulus G_0 , the average values of about 41 and 21 MPa were obtained for the soft (test DG01) and very soft (test DG03) tests, respectively, while average values of the undrained shear strength s_u were equal to about 43 and 6 kPa (Tab. 1). The experimental results were compared with values provided by some empirical relations available in the literature, such as those by Azeiteiro *et al* (2017) and Hardin & Drnevich (1972) for the small-strain shear modulus G_0 and the one from Wroth (1984) for the undrained shear strength s_u . The best agreement with the experimental results was obtained for the DG03 test in terms of soil stiffness, while a good accordance was observed for both tests in terms of strength.

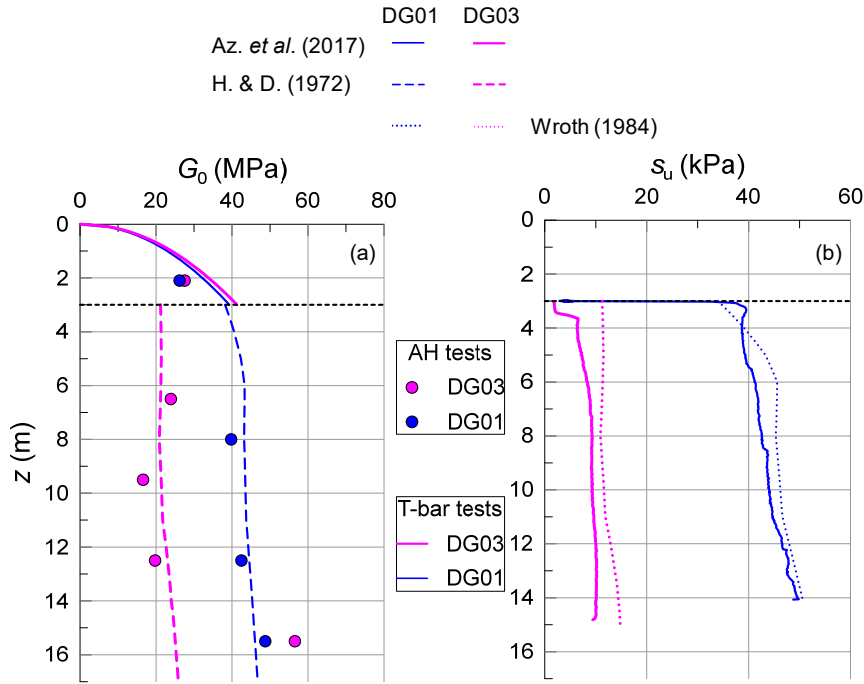


Figure 4. Experimental and empirical (a) small-strain shear modulus and (b) undrained shear strength profiles

Table 1. Average mechanical properties of the far-field soil column in the two centrifuge tests

test	G_0 (MPa)	s_u (kPa)
DG01	41.2	43.3
DG03	26.6	6.4

In both tests DG01 and DG03, the system was subjected to several real and sinusoidal seismic inputs. Here the results obtained applying the seismic input recorded during the destructive Christchurch (2011) earthquake are discussed; its amplitude was scaled to obtain a weak ($a_x^{\text{inp}} = 0.030g$, Fig. 6d), a moderate ($a_x^{\text{inp}} = 0.100g$, Fig. 7d), and a strong ($a_x^{\text{inp}} = 0.212g$, Fig. 8d) version of the seismic record. The first and the third base excitations were applied to the base of the weak clay (DG03), while the second one to the base of the stronger clay (DG01), so as to study the influence of the seismic intensity on the system performance. The ground motions were imposed at the base of the ESB box through the servo-hydraulic shaker described by Madabhushi *et al* (2012).

EXPERIMENTAL RESULTS

In this section, the results obtained applying the seismic inputs mentioned above are discussed, first referring to the far-field soil response and then to the seismic behaviour of the whole soil-caisson-pier-deck system.

Far-field soil response

The far-field soil response is given in Figure 5, where the shear stress-shear strain loops obtained at depth $z = 6.5$ m, which is close to the caisson base, is given for all cases considered in this paper, namely the weak input + weak soil (i.e. very soft clay, DG03 test, Fig. 5a), the moderate input + strong soil (i.e. soft clay, DG01, Fig. 5b), and the strong input + weak soil (i.e. very soft clay, DG03, Fig. 5c). In the first case, low seismic-induced shear strains ($\gamma_{\text{max}} = 2.5 \cdot 10^{-3}$) were mobilised, which were accompanied by quite a narrow loop area and consequent nearly null energy dissipation: in this case, the induced shear stress τ in the soil is far from the limit shear stress, $\tau_{\text{max}} = s_u$. Vice versa, the third case (Fig. 5c), ruled by the high seismic intensity travelling

into a weak clay deposit, shows an almost tripled peak shear strain ($\gamma_{\max} = 7.0 \cdot 10^{-3}$) together with a much broader loop area, which indicates a remarkable soil hysteretic damping: this time, the undrained shear strength is attained, limiting the shear stress τ that can be transmitted to the upper portion of soil deposit. The moderate input + strong soil (Fig. 5b) locates in the middle between the two extreme cases, showing a peak shear strain γ_{\max} which is comparable to that mobilised in the strong input case, although not triggering soil shear strength.

Therefore, the first case (Fig. 5a) can be seen as representative of an elastic case, whereas the second (Fig. 5b) and the third ones (Fig. 5c) can be viewed as cases where soil inelastic behaviour is slightly and strongly mobilised, respectively, mainly due to the interaction between the increasing amplitude of the seismic shaking and the varying shear strength of the soil. This interplay will be influencing the seismic performance of the entire soil-caisson-pier-deck system, as discussed in the next section.

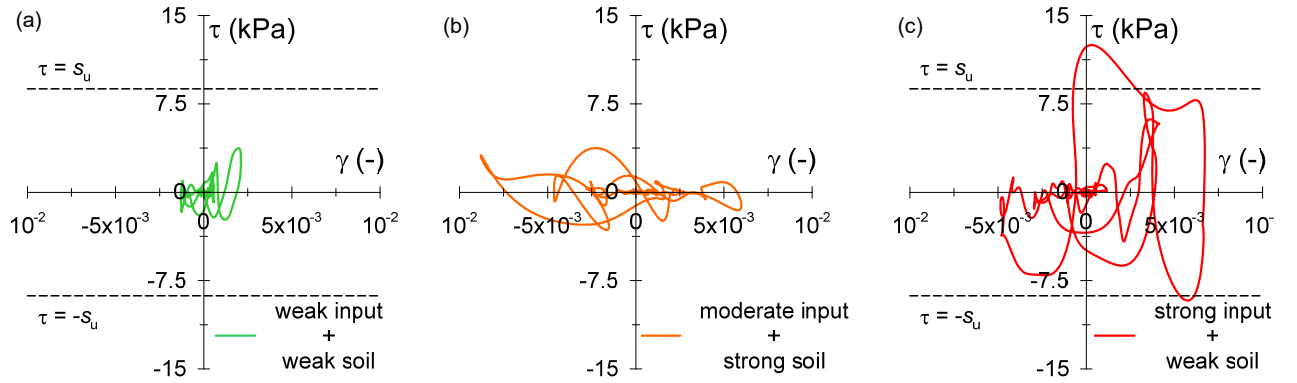


Figure 5. Far-field shear stress-shear strain loops (depth $z = 6.5$ m) for increasing amplitude of the scaled Christchurch motion: (a) weak input on weak soil (test DG03); (b) moderate input on strong soil (test DG01); (c) strong input on weak soil (test DG03)

Seismic behaviour of the system

The seismic behaviour of the system at hand was quantified in terms of the nondimensional deck drift u_{rel}/h_s and of the bending moment acting at the base of the pier, M_s . The deck drift is defined as

$$u_{\text{rel}} = u_{\text{deck}} - u_{\text{caisson head}} = \tan \theta \cdot h_s + u_{\text{flex}} = u_{\text{rel, rigid}} + u_{\text{flex}} \quad (3)$$

where u_{deck} and $u_{\text{caisson head}}$ are the horizontal displacements of the deck and the top of the caisson, θ is the rigid caisson rotation, $u_{\text{rel, rigid}}$ is the rigid component of the drift and u_{flex} is the elastic bending of the pier, that is the one directly related to the bending moment M_s . The latter has been computed as

$$M_s = m_{\text{eff}} \cdot a_{\text{deck}} \cdot h_s \quad (4)$$

where $m_{\text{eff}} = 270.43$ Mg is the effective mass related to the first mode of the fixed-base pier. The time histories of horizontal displacement were computed through double integration of the ones of average acceleration as obtained from MEMS M_{1-2} and M_{5-6} , while the time history of the rigid rotation θ was computed as $\theta = [w_{L3} - w_{L2}]/d$, where w indicates the caisson settlement and d is the distance between LVDTs $L_{2,3}$. All results presented hereafter are at the prototype scale, unless otherwise specified.

The observed time histories of drift and bending moment are plotted in Figures 6, 7, and 8 for the three increasing amplitudes of the ground motion. In the weak input + weak soil case (Fig. 6), no permanent drift is obtained ($u_{\text{rel, rigid}}/h_s = 0$) due to the very low intensity of the input motion. This result is consistent with the *far-field* shear stress-shear strain loop computed at a depth $z = 6.5$ m (Fig. 5a). This outcome also allows to state that soil response is about elastic when subjected to the weak ground motion.

With increasing seismic amplitude (test DG01), the system starts accumulating a permanent rigid rotation (Fig. 7b). However, this is still relatively small ($u_{rel, rigid}/h_s = -0.18\text{‰}$) as a consequence of the higher undrained shear strength measured along the *far-field* alignment. Hence, in this test, irreversible soil behaviour influenced the system response only very slightly, while still limiting the inertial forces transmitted to the superstructure; indeed, despite the input amplitude increased more than three times (ratio between $a_x^{inp_{max}}$ equal to $0.102/0.030 = 3.4$), the increment obtained in the peak values of the deck drift, u_{rel} , was only 33 % and the maximum bending moment, M_s , increased by 70 %.

Conversely, in the case of the strong seismic input applied to the weak soil, a strong increase of the permanent rotation was accumulated by the system, which is tripled ($=0.60\text{‰}$, Fig. 8b). Nonetheless, the bending moment turned out to be lower than that attained by the moderate input on the strong soil case (Fig. 8c), which decreased by about 32 %, despite the input amplitude doubled. The peak bending moment attained in this case ($M_{s, max} = 11.37\text{ MN}\cdot\text{m}$) is limited by the soil-caisson capacity, as discussed in the following section. It is therefore apparent that the irreversible and hysteretic soil behaviour is contributing to reduce the inertial forces transmitted to the superstructure, governing the system seismic performance. This is also clear from the noticeable period elongation of both the time histories of deck drift and bending moment plotted in Figure 8.

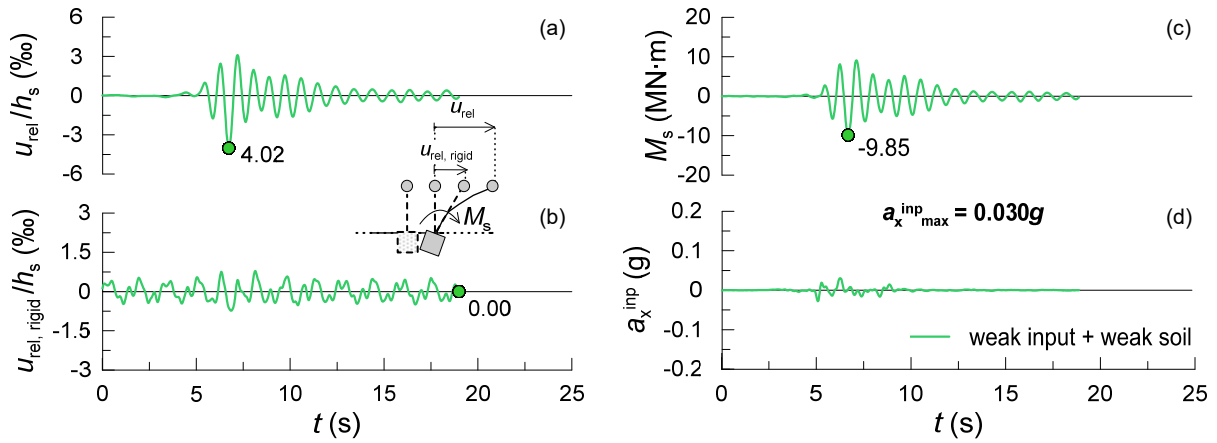


Figure 6. Time histories of the (a) total and (b) rigid component of the deck drift, (c) bending moment and (d) horizontal acceleration of the weak input motion on weak soil (DG03)

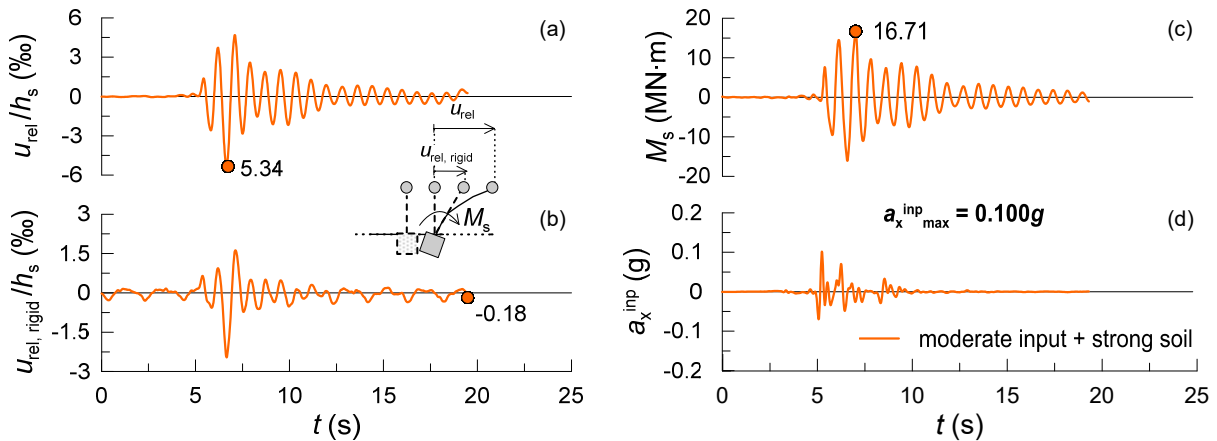


Figure 7. Time histories of the (a) total and (b) rigid component of the deck drift, (c) bending moment and (d) horizontal acceleration of the moderate input motion on strong soil (DG01)

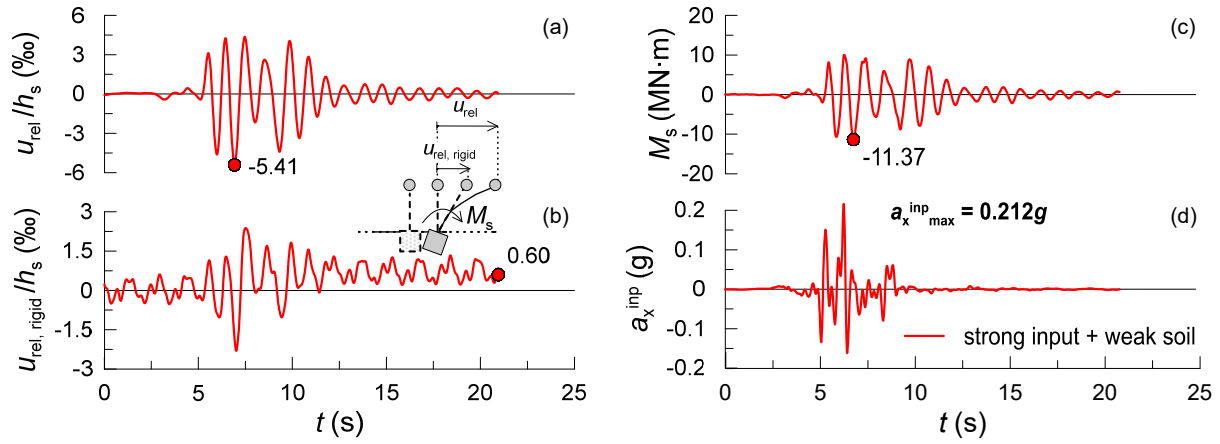


Figure 8. Time histories of the (a) total and (b) rigid component of the deck drift, (c) bending moment and (d) horizontal acceleration of the strong input motion on weak soil (DG03)

ASSESSMENT OF SEISMIC PERFORMANCE

From the seismic behaviour discussed in the previous section, it follows that the system response was assessed referring to some performance indexes, such as the peak and permanent values of the nondimensional deck drift, $u_{rel,max}/h_s$ and $u_{rel,perm}/h_s$, and the peak bending moment $M_{s,max}$, which are plotted in Figure 9 against the peak acceleration of the seismic shaking, $a_x^{inp,max}$. This shows that all quantities increase in the low-intensity range (i.e. $a_x^{inp,max} \leq 0.1$ g) for increasing amplitudes, as expected. Conversely, the peak deck drift almost stabilises while the peak bending moment even decreases in the moderate-to-high intensity range ($a_x^{inp,max} > 0.1$ g), being limited by the attainment of the soil-caisson resistance. The latter was estimated using the empirical relations provided for clays by Gerolymos *et al* (2015) and Rosati *et al* (2022), the first developed through a total stress approach, while the second with an effective stress approach. Their evaluation of the limit bending moment acting at the base of the pier, causing the bearing capacity mechanism to occur, $M_{s,f}$, is equal to 12.5 and 14.9 MN·m, respectively, being in a good agreement with the value obtained in the centrifuge ($M_{s,max} = 11.37$ MNm) for the test DG03 with $a_x^{inp,max} = 0.212$ g. Higher values of $M_{s,max}$, lying in between the two limit values $M_{s,f}$, have been obtained when applying other seismic inputs (not shown in this paper for the sake of space), which confirms that the actual limit value might be located in between them (Gaudio *et al.*, 2022b).

Opposite to what observed for the peak values, the permanent deck drift shows an almost linear increase with the seismic intensity, which confirms the growing role of inelastic soil behaviour on the seismic performance of the system as the seismic amplitude increases.

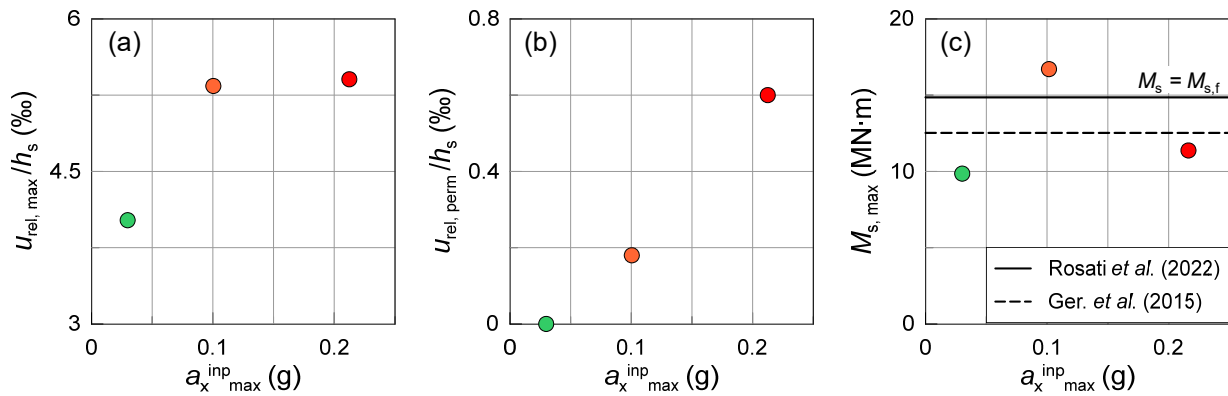


Figure 9. Seismic performance against the peak acceleration of the seismic input: (a) peak and (b) permanent nondimensional deck drift; (c) peak bending moment

CONCLUDING REMARKS

This paper illustrated a preliminary interpretation of the results obtained from dynamic centrifuge tests of caisson foundations supporting bridge piers subjected to weak, moderate and strong ground motions. The discussion mainly showed that the inelastic and hysteretic behaviour of the foundation soil can play a fundamental role in the seismic performance of the whole system; this is particularly true for strong seismic events, for which the soil acts as a “fuse”, thus limiting the inertial forces transmitted to the superstructure.

Further elaboration of the discussed results is of course needed, *e.g.*, to understand and quantify the relative contribution of the free-field and near-field hysteretic soil behaviour, considering also the remaining seismic inputs applied in the centrifuge tests.

REFERENCES

- Azeiteiro RJN, Coelho PALF, Taborda DMG, Grazina JCD (2017). Critical State-Based Interpretation of the Monotonic Behaviour of Hostun Sand. *Journal of Geotechnical and Geoenvironmental Engineering*, ASCE, 143(5), 04017004.
- Brennan AJ & Madabhushi SPG (2002). Design and performance of a new deep model container for dynamic centrifuge testing. *Proc. Int. Conf. on Phys. Mod. Geotech.*, Balkema, Rotterdam, The Netherlands, St Johns NF, Canada, (pp. 183-188).
- Garala TK & Madabhushi SPG (2019). Seismic behaviour of soft clay and its influence on the response of friction pile foundations. *Bulletin of Earthquake Engineering* 17(4), pp. 1919-1939.
- Gaudio D, Madabhushi SPG, Rampello S & Viggiani GMB (2022b). Experimental investigation of the seismic performance of caisson foundations supporting bridge piers, *Géotechnique* (submitted for publication)
- Gaudio D & Rampello S (2019a). The influence of soil plasticity on the seismic performance of bridge piers on caisson foundations. *Soil Dynamics and Earthquake Engineering*, 118, pp. 120-133. <https://doi.org/10.1016/j.soildyn.2018.12.007>
- Gaudio D & Rampello S. (2019b). The role of soil constitutive modelling on the assessment of seismic performance of caisson foundations. *Proc. 7th Int. Conf. Geot. Earthq. Eng.*, Rome, Italy, (pp. 2574-2582) <https://doi.org/10.1201/9780429031274>
- Gaudio D & Rampello S (2021). On the assessment of seismic performance of bridge piers on caisson foundations subjected to strong ground motions. *Earthquake Engineering & Structural Dynamics*, 50(5), pp. 1429-1450. <https://doi.org/10.1002/eqe.3407>
- Gaudio D, Seong J, Haigh SK, Viggiani GMB, Madabhushi SPG, Shrivatsava R, Veluvolu R, Padhy P (2022a). Boundary effects on dynamic centrifuge modelling of onshore wind turbines on liquefiable soils, *International Journal of Physical Modelling in Geotechnics* (accepted for publication)
- Gazetas G (2015). 4th Ishihara lecture: soil–foundation–structure systems beyond conventional seismic failure thresholds. *Soil Dynamics and Earthquake Engineering* 68, pp. 23-39.
- Gerolymos N, Zafeirakos A, Karapiperis K (2015). Generalized failure envelope for caisson foundations in cohesive soil: Static and dynamic loading. *Soil Dynamics and Earthquake Engineering* 78, pp. 154-174.
- Ghosh B & Madabhushi SPG (2002). An efficient tool for measuring shear wave velocity in the centrifuge. *Proc. Int. Conf. Phys. Mod. Geotech.* (eds R. Phillips, P. J. Guo and R. Popescu), Balkema, Rotterdam, The Netherlands, (pp. 119–124).
- Hardin BO & Drnevich VP (1972). Shear modulus and damping in soils: design equation and curves. *J. Soil Mech. Found. Eng. Div.* 98(SM7), pp. 667–692.
- Madabhushi SPG, Haigh SK, Houghton NE Gould E (2012). Development of a Servo-Hydraulic Earthquake Actuator for the Cambridge Turner Beam Centrifuge. *International Journal of Physical Modelling in Geotechnics* 12, No. 2, 77-88.
- Rosati A, Gaudio D, di Prisco CG, Rampello S (2022). Use of interaction domains for a displacement-based design of caisson foundations, *Acta Geotechnica* (under revision)
- Sakellariadis L, Anastasopoulos I, Gazetas G (2020). Fukae bridge collapse (Kobe 1995) revisited: New insights. *Soils and Foundations* 60 (6), pp. 1450-1467.
- Stewart DP & Randolph MF (1991). A New Site Investigation Tool for the Centrifuge. *Proc. Int. Conf. Centr. Mod., Centrifuge '91*, Boulder, Colorado, 13-14 June 1991, Balkema, Rotterdam, the Netherlands, (pp. 531-538).
- Wroth CP (1984). The Interpretation of In Situ Soil Tests. *Geotechnique* 34(4), pp. 449–489.